IEEE Access
Multidisciplinary | Rapid Review | Open Access Journal

Received May 15, 2019, accepted June 22, 2019, date of publication June 26, 2019, date of current version July 12, 2019.

Digital Object Identifier 10.1109/ACCESS.2019.2925196

Defect Detection for Patterned Fabric Images Based on GHOG and Low-Rank Decomposition

CHUNLEI LI[1], GUANGSHUAI GAO[1,2], ZHOUFENG LIU[1], DI HUANG[2], (Member, IEEE), AND JIANGTAO XI[3], (Senior Member, IEEE)

[1]Electronic and Information Engineering, Zhongyuan University of Technology, ZhengZhou 450007, China
[2]Computer Science and Engineering, Beihang University, Beijing 100191, China
[3]Electrical, Computer, and Telecommunications Engineering, University of Wollongong, Wollongong, NSW 2522, Australia

Corresponding author: Chunlei Li (lichunlei1979@sina.com)

This work was supported in part by the National Natural Science Foundation of China under Grant U1804157 and Grant 61772576, in part by the Key Natural Science Foundation of Henan Province under Grant 162300410338, in part by the Science and Technology Innovation Talent Project of Education Department of Henan Province under Grant 17HASTIT019, in part by the Henan Science Fund for Distinguished Young Scholars under Grant 184100510002, in part by the Henan Science and Technology Innovation Team under Grant CXTD2017091 and Grant IRTSTHN(18IRTSTHN013), and in part by the Program for Interdisciplinary Direction Team in Zhongyuan University of Technology.

ABSTRACT In contrast to defect-free fabric images with macro-homogeneous textures and regular patterns, the fabric images with the defect are characterized by the defect regions that are salient and sparse among the redundant background. Therefore, as an effective tool for separating an image into a redundant part (the background) and sparse part (the defect), the low-rank decomposition model provides an ideal solution for patterned fabric defect detection. In this paper, a novel patterned method for fabric defect detection is proposed based on a novel texture descriptor and the low-rank decomposition model. First, an efficient second-order orientation-aware descriptor, denoted as GHOG, is designed by combining Gabor and histogram of oriented gradient (HOG). In addition, a spatial pooling strategy based on human vision mechanism is utilized to further improve the discrimination ability of the proposed descriptor. The proposed texture descriptor can make the defect-free image blocks lay in a low-rank subspace, while the defective image blocks have deviated from this subspace. Then, a constructed low-rank decomposition model divides the feature matrix generated from all the image blocks into a low-rank part, which represents the defect-free background, and a sparse part, which represents sparse defects. In addition, a non-convex log det as a smooth surrogate function is utilized to improve the efficiency of the constructed low-rank model. Finally, the defects are localized by segmenting the saliency map generated by the sparse matrix. The qualitative results and quantitative evaluation results demonstrate that the proposed method improves the detection accuracy and self-adaptivity comparing with the state-of-the-art methods.

INDEX TERMS Patterned fabric, defect detection, GHOG, low-rank decomposition, ADMM.

I. INTRODUCTION

Fabric defect detection is the key step in quality control of textile products. Currently, it is mainly conducted visually by skilled workers. However, the detection accuracy and reliability are restricted by the human errors and eye fatigue. Automatic and intelligent detection and analysis of fabric defects based on machine vision can provide a promising solution, which not only minimizes labor costs, but also improves accuracy and efficiency. With the development of machine vision technology, some fabric inspection machines have been successfully applied to the textile process, such as Shelton web-SPECTOR, Barco Visions Cyclops, EVS ITex2000 and MQT. However, these inspection systems only work for limited fabric types. Therefore, it is necessary to further study the fabric defect detection methods.

Machine vision based methods for fabric defect detection should be designed based on the features of fabric images, e.g., their texture. One feature is the pattern, referring to the unit repetitively shown on the fabric. Fig. 1 shows the fabrics with different patterns from simple non-motif patterns (twill and plain fabrics, as shown in Fig. 1(a)) to the complex motif

The associate editor coordinating the review of this manuscript and approving it for publication was Auday A.H. Mohamad.

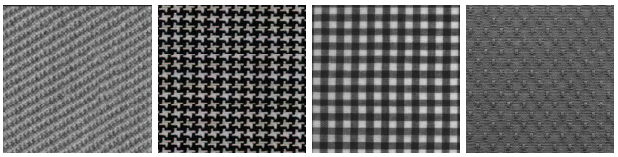

(a) (b) (c) (d)

FIGURE 1. (a) Plain and twill. (b) Star-patterned fabric. (c) Box-patterned fabric. (d) Dot-patterned fabric.

patterns (e.g., dots, boxes, and stars as shown in Fig. 1(b-d)). For the plain and twill fabrics, the background is homogeneous and the defects are salient. Therefore, it is relatively easy to detect defects on these fabrics. Most exiting methods were designed for plain and twill fabrics and can achieve high detection rate for this type of fabrics. These approaches can be classified into four categories, including statistical analysis methods [1], frequency transform methods [2], model based methods [3], and dictionary learning methods [4]. However, these methods do not work well for fabrics with complex patterns due to a few challenges. This is because the repetitive unit has a complex structure, which can be similar to the defects, making the detection difficult. Besides, it is difficult to collect the data samples of defects on these complex fabrics for the construction of available benchmark datasets.

Recently, a few methods have been proposed for the fabrics with complex patterns, such as the ELO rating (ER) method [5], and wavelet-preprocessing golden image subtraction (WGIS) [6]. These approaches also suffer from some advantages, e,g., requiring non-defective samples. In addition, the accuracy of these methods heavily relies on the accurate partitions and the selected template.

Low-rank decomposition model is an effective method that divides a data matrix into a redundant part spanning several low-rank subspaces and a sparse part which is the outlier [7]. As the method can simultaneously detect the outliers and recovers the low-dimensional subspace of matrices, it has been successfully applied for the problems of object detection, image segmentation, image denoising, etc. For patterned fabric images, the defect-free regions are macro-homogeneous, which lay in a low-dimensional subspace, while the defective regions are salient and sparse. Therefore, low rank decomposition model can be an effective tool for the task of the patterned fabric defect detection.

However, directly using low-rank decomposition in the raw pixel space of images to detect defects in the complex patterned fabrics is not practical due to the low accuracy. This promotes us to introduce new powerful descriptors to efficiently characterize the fabric texture, which make the defect-free or background regions lay in a low rank subspace, whilst the defective regions deviate from the subspace. In order to efficiently characterize the fabric texture, the following should be considered: 1) Texture of defect-free fabric images usually has specific layout in a unique orientation, yet the appearance of defects damages the regularity of this orientation. Therefore, an orientation-aware descriptor should be used for representing the fabric image features; 2) Due to the complex texture of the fabric images, the gray value exhibits a high frequency variance, and hence a high order gradient descriptor should be employed rather than the first-order gradient descriptor.

In this paper, we propose to use a second-order orientation-aware descriptor, denoted as GHOG, by combing Gabor and HOG. As the 2-dimensional (2D) Gabor transform are similar to biological visual sensory systems that can efficiently extract the orientation, it is used to generate the first-order orientational maps. Then, we use them as the inputs to calculate the second order gradient orientational map over the same image region. Thereafter, HOG is generated by counting the gradient magnitude when the gradient orientation is consistent with the orientation of Gabor filtered maps. In addition, in order to further enhance the ability of the describing large variety of local shape changes and to increase discrimination ability, a spatial pooling strategy is embedded into the model. Then, an efficient low-rank decomposition model is constructed to divide the matrix generated by the orientation feature extracted from image blocks into a low-rank matrix (background information) and a sparse matrix (defect information). In addition, a non-convex log det is utilized as a smooth surrogate function to accelerate the convergence speed of the constructed low-rank model. Finally, the defects are localized by segmenting the saliency map generated by the sparse matrix.

A preliminary conference version of this work has been published in [8]. This paper includes the work in [8] but significantly extends it in the following points: 1) In [8], the traditional HOG was used to extract the feature from Gabor maps. In this paper, HOG is generated by counting the gradient magnitude when the gradient orientation is consistent with the orientation of Gabor filtered maps; 2) Following the idea of [8], a spatial pooling strategy is utilized to enable small displacement of second order gradients in the neighborhood of a certain point; 3) A non-convex log det is also exploited as a smooth surrogate function for the rank instead of the nuclear norm to improve the efficiency of the low-rank model; 4) Experimental results are presented to further demonstrate the efficiency of our proposed method.

The reminder of this paper is organized as follows. Section II introduces the related work of fabric defect detection. In Section III, the proposed algorithm is presented. Section IV gives evaluation on the performance of the proposed algorithm in comparison with other existing methods. Finally, we conclude the paper in Section V.

II. RELATED WORK

Many methods of fabric defect detection were proposed with the aim to improve the accuracy and to reduce the computational complexity. Most proposed methods are generally used to detect defects in plain and twill fabrics, and they mainly include four categories: spectral analysis, model-based, and dictionary learning approaches. Spatial statistical methods via calculating gray-scale values of the defects

contrasted with their surroundings, including histogram character analysis method [9], local contrast enhancement method [10]. However, these methods heavily rely on the size of selected windows and their discrimination rules. Moreover, they always suffer from the issue to detect small size defects.

With spectral analysis methods, an image of interest is converted into spectral domain using a suitable orthogonal transform, e.g, the Fourier transform (FT) [11], the Gabor transform [12] and the orthogonal wavelet transform [2]. However, these methods require huge amount of computations and hence are not efficient.

Model-based methods extract texture features by means of modeling and parameter estimation. Defect detection is realized by estimating whether the test image is consistent with the model with normal textures. A few model-based methods were reported, such as Gaussian-Markov random field (GMRF) [13], and Gaussian mixture model (GMM) [14]. These methods can achieve satisfactory performance, but they usually suffer from high computational complexity, and also the model-based methods cannot efficiently detect the defects of smaller size.

With dictionary learning based methods, defects are located in two ways: one is first to construct a dictionary by adaptively learning the training or test images, and then reconstruct the defect-free fabric image based on this dictionary. The defects are identified by subtracting the reconstructed image from the input test image [15]. The other is to construct a dictionary in the same way, and then the image patch to be tested is projected on to the dictionary, leading to reduction in the dimension of the image patch. The defects are detected using the support vector data description (SVDD) technique [16]. However, these two methods requires construction of a dictionary for every type of textile images, and thus are not efficient in terms of computational burden. Also the performance of the first method may suffer from the problem that the reconstructed images may exhibit areas similar to defects.

For complicated patterned fabrics, several methods have been recently published, such as the wavelet pre-processing golden image subtraction (WGIS) [6], template matching for discrepancy measures (TMPM) [17], the Bollinger bands (BB) [18], the regular bands (RB) [19] and the ELO rating method [5].

With WGIS, a template (also called golden image) is selected from defect-free images. Both the template and the images to be tested are pre-processed by wavelet filtering. Then the defects are detected by evaluating the difference between the pre-processed template and the test images. The TMPM method also makes use of a golden image as the template for defect detection, but it uses a fitness function to explore the difference between the template and the images to be tested. The BB and RB methods detect the defects by comparing the moving averages and standard deviations of small area of images against certain thresholds obtained from the regularity property of a patterned texture, e.g., dot-, boxand star-patterned fabrics. ELO rating (ER) define a similarity which named as competition score between two image blocks. The defective image block are detected by calculating the score between the test image block and a trained template.

The above techniques for patterned fabric defect detection employs traditional methods to characterize the fabric texture, such as wavelet transform, Gabor transform, average value, and standard deviation. A common feature of patterned fabric images is the normal background with certain orientation, which will be destroyed by the defects. Therefore, the orientation is an important feature for describing the fabric texture. In addition, as fabric images have the complex texture and complex variations in their grey level, high-order gradient should be used to describe them. However, the existing methods did not consider these characteristics of the patterned fabric image. On the other hand, the majority of existing methods for complicated pattern usually utilize template matching techniques to localize the defective regions. The detection accuracy depends on precise alignment and selection of a suitable template.

By decomposing the feature matrix into a low-rank matrix corresponding to the background and a sparse matrix corresponding to the object, low-rank decomposition model can be well applied for the patterned fabric defect detection problem [20]–[22]. However, the performance of the low-rank decomposition model depends on selection of a descriptor. An efficient descriptor can make the background part in a lower dimensional feature subspace, and the sparse part is more far away from the subspace. Therefore, an effective feature extraction is the crucial step for low-rank decomposition.

In this paper, we propose a powerful second order orientation aware descriptor, denoted as GHOG, for characterizing the fabric texture. Moreover, an effective low rank decomposition model is introduced to separate the defective regions from the normal background.

III. THE PROPOSED ALGORITHM

In this section, we describe the proposed fabric defect detection method, which includes feature extraction of GHOG descriptor, construction of low-rank decomposition model, optimization of the model and acquisition and segmentation of the saliency map.

A. FEATURE EXTRACTION OF GHOG

Effective fabric defect detection requires powerful feature descriptors, characterized by uniqueness in measurements, and thus sufficient discriminative capabilities. Considering the aforementioned characteristics of patterned fabric image, a second order orientation-aware descriptor is a suitable tool for describing complex texture. Therefore, GHOG, a new feature descriptor is proposed, leading to reduction in the dimension of the feature vectors and capturing information of second order orientation. The proposed GHOG descriptor is shown in Fig. 2, and the detailed procedures are described as follows:

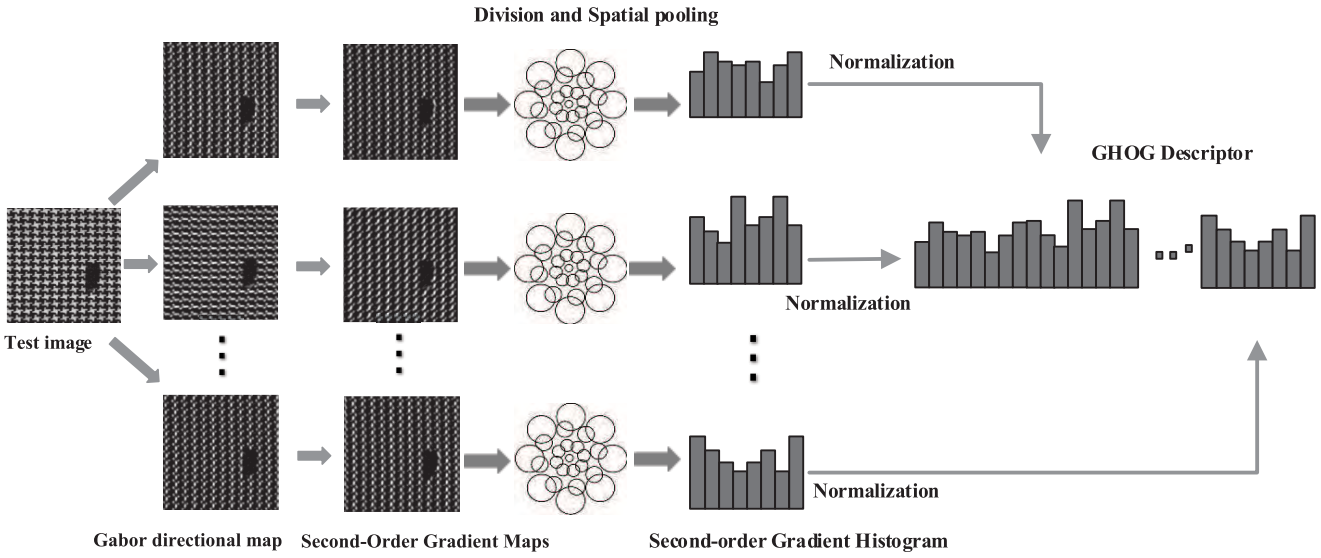

FIGURE 2. Feature extraction of GHOG.

1) **Gabor orientational filtered map generation.** The 2-D Gabor filter has the following complex form [23]:

$$g(x, y; \lambda, \psi, \sigma, \gamma) = \exp\left(-\frac{x'^2+\gamma^2 y'^2}{2\sigma^2}\right)\exp\left(i\left(2\pi\frac{x'}{\lambda}+\psi\right)\right) \tag{1}$$

Its real part is:

$$g(x, y; \lambda, \psi, \sigma, \gamma) = \exp\left(-\frac{x'^2+\gamma^2 y'^2}{2\sigma^2}\right)\cos\left(2\pi\frac{x'}{\lambda}+\psi\right) \tag{2}$$

And its imaginary part is described as:

$$g(x, y; \lambda, \psi, \sigma, \gamma) = \exp\left(-\frac{x'^2+\gamma^2 y'^2}{2\sigma^2}\right)\sin\left(2\pi\frac{x'}{\lambda}+\psi\right) \tag{3}$$

where $x' = x\cos\theta + y\sin\theta$, $y' = -x\sin\theta + y\cos\theta$, λ is wave length, which is not smaller than 2, and no more than 1/5 of the size of the input image; θ denotes the orientation, whose value ranges from 0 to 2π; ψ represents phase shift ranging from $-\pi$ to π, while 0 and π respectively correspond to center-on and center-off functions, and $-\pi/2$ and $\pi/2$ correspond to anti-symmetric function; γ is the length-to-width ratio of the filter, which determines the ellipticity of the Gabor function; the shape is round when $\gamma = 1$, and the shape stretches along the orientation of parallel stripes when $\gamma < 1$. In this paper, γ is set to 0.5; σ is the standard deviation of the Gaussian factor in the Gabor function. The value of σ cannot be preset directly, as it depends on the bandwidth b. b must be a positive constant, which is related to the ratio of σ/λ, i.e., $b = \log_2 \frac{\frac{\sigma}{\lambda}\pi+\sqrt{\frac{\ln 2}{2}}}{\frac{\sigma}{\lambda}\pi-\sqrt{\frac{\ln 2}{2}}}$, $\frac{\sigma}{\lambda} = \frac{1}{\pi}\sqrt{\frac{\ln 2}{2}}\cdot\frac{2^b+1}{2^b-1}$. In this paper, we usually set $b = 1$, and then the relationship of σ and λ is $\sigma = 0.56\lambda$.

In this paper, we choose eight orientations $\theta(\theta = 0^0, 45^0, 90^0, 135^0, 180^0, 225^0, 270^0, 315^0)$ with one scale to filter the patterned fabric image, and accordingly eight **directional filtered maps** G_o ($o = 1, 2, \ldots, K$, K is set to 8 in this paper) are generated to capture the orientational features as follows.

$$G_k(x, y) = \sqrt{(G_{R_k}(x, y) * I(x, y))^2 + (G_{I_k}(x, y) * I(x, y))^2} \tag{4}$$

where $I(x, y)$ represents the input image, $G_{R_k}(x, y)$ and $G_{I_k}(x, y)$ for the real and imaginary part of the Gabor filter in the $k-th$ orientation, '*' represents convolution operation.

2) **Generation of the Second-Order Gradient Orientational Maps.** After generating the first order orientational filtered map $G_k(x, y)$, we use them as the inputs to calculate the second order gradient orientational map over the same image region.

First of all, the gradients in the horizontal and vertical directions of the image pixel are calculated as follows:

$$GM_k(x, y) = \sqrt{\left(\frac{\partial G_k(x, y)}{\partial x}\right)^2 + \left(\frac{\partial G_k(x, y)}{\partial y}\right)^2} \tag{5}$$

$$\theta_k(x, y) = \arctan\left(\frac{\partial G_k(x, y)}{\partial y} \Big/ \frac{\partial G_k(x, y)}{\partial x}\right) \tag{6}$$

$$\frac{\partial G_k(x, y)}{\partial x} = G_k(x+1, y) - G_k(x-1, y) \tag{7}$$

$$\frac{\partial G_k(x, y)}{\partial y} = G_k(x, y+1) - G_k(x, y-1) \tag{8}$$

Then each orientation is mapped to the range of $[0, 2\pi]$ from that of $[-\pi/2, \pi/2]$, which keeps consistent with the number of the Gabor filter maps. After quantization, the entry n_o of each orientation θ_o is computed as follows:

$$n_o(x, y) = \mathrm{mod}\left(\left\lfloor\frac{\theta_o(x, y)}{2\pi/N}+\frac{1}{2}\right\rfloor, N\right), \quad o = 1, 2, \ldots, K \tag{9}$$

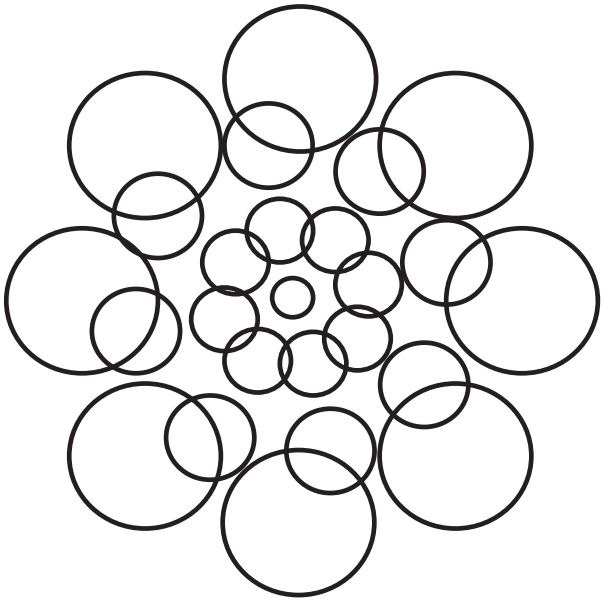

FIGURE 3. The Spatial pooling arrangement of the proposed GHOG descriptor.

Then, the second-order gradient magnitude $GM_k(x, y)$ is used as pixel value to generate the second-order gradient map for each pixel location (x, y).

3) **Spatial pooling.** After generating the second-order orientation map $GM_k(x, y)$, we employ spatial pooling to generate the local descriptor. Firstly, we equally divided the input image $GM_k(x, y)$ into N blocks $GM_k^i(x, y)$, $i = 1, 2, ..N$ with the same size $N_b \times N_b$, and N_b is set to 16 in this paper; then each image block is divided into sub-regions using spatial pooling strategy, and a histogram of certain property (such as edge points, gradients and binary patterns) is generated for each sub-region. In the end, the final descriptor for each image block is formed by concatenating all these histograms of all the orientations. As suggested by Brown *et al.* [24], DAISY-style operation achieved the best performance by comparing several different spatial pooling strategies. Therefore, we adopt this strategy to build our proposed GHOG descriptor. The strategy is illustrated in Fig. 3.

As shown in Fig. 3, on the input image block, a series of concentric rings of concentric rings is marked whose radius are arranged in arithmetic sequence. On each ring, we have K circles with its centers evenly distributed, and the radius of the circles is proportional to the radius of the ring. Therefore, there are four parameters which determine the spatial arrangement of the GHOG descriptor: the number of quantized orientations (K); the radius of the region (R); the number of circles on each ring (C); the number of concentric rings (CR). We empirically set R = 8, K = 8, CR = 3 and C = 8 in our case.

The total number of the decomposed circles can be computed as $T = CR \times C + 1$. Within each circle CRI_j, $j = 1, 2, \ldots T$ and for each image block GM_k^i, we define $H_{kj}(s)$ as the histogram of orientation gradients features of GM_k^i, which is constructed by accumulating the gradient magnitude GM_k^i of all the pixels with the same quantized orientation entry n_k.

$$H_{kj}^i(s) = \sum_{(x,y)\in CRI_j} f(n_k(x, y) = s) * GM_k^i(x, y) \quad (10)$$

where $s = 0, 1, \ldots, K-1$; $k = 1, 2, \ldots, K$; $j = 1, 2. \ldots, T$.

$$f(X) = \begin{cases} 1, & if\ X\ is\ true \\ 0, & otherwise \end{cases} \quad (11)$$

Next, for each block of second-order orientation map, we concatenate all the histograms from T circles (as shown in Fig. 3) to obtain its second order gradient histogram H_k^i.

$$H_k^i = [H_{j1}^i, H_{k2}^i, \cdots, H_{kT}^i]^T \quad (12)$$

Then, normalize each histogram H_k^i to a unit norm vector$\widehat{H}_k^i$:

$$\widehat{H}_k^i = \frac{H_k^i}{\|H_k^i\|} \quad (13)$$

where $\|\cdot\|$ usually stands for ℓ_2-norm.

For each block of second order gradient maps GM_k^i, its GHOG features $GHOG_i$ is generated by concatenating the histograms of all the orientations.

$$GHOG_i = \left[\hat{H}_1^i, \hat{H}_2^i, \ldots, \hat{H}_K^i\right]^T \quad (14)$$

In order to construct the model in the following section, we define a feature matrix $\mathbf{F}$ as the final GHOG descriptors to represent the information of the entire image.

$$F = [GHOG_1, GHOG_2, \ldots, GHOG_N] \quad (15)$$

B. CONSTRUCTION OF LOW-RANK DECOMPOSITION MODEL

After obtaining the feature matrix $\mathbf{F}$, the problem of fabric detection is to use an effective model to decompose the feature matrix $\mathbf{F}$ into a redundant information part $\mathbf{L}$ (non-salient background) and a sparse part $\mathbf{S}$ (salient defect). And the low-rank decomposition model is formulated as:

$$(L^*, S^*) = \arg\min_{(L,S)} (rank(L) + \mu \|S\|_0)\ s.t. F = L + S \quad (16)$$

where L lies in the low-rank subspace, representing the normal background, that is, the regularly repetitive texture. S lies in the sparse subspace, and represents the defective regions.

Since Eq. (14) is non-deterministic polynomial (NP)-hard problem, it is difficult to obtain the optimal solution of Eq. (13). We utilize the following convex function to surrogate it:

$$(L^*, S^*) = \arg\min_{(L,S)} (\|L\|_* + \mu \|S\|_1)\ s.t. F = L + S \quad (17)$$

where $\|L\|_*$ is the nuclear norm of $\mathbf{L}$, which is the sum of the singular values of $\mathbf{L}$; $\|.\|_1$ indicates the l_1 norm, which is the sum of absolute value of all the elements in each column vector; μ is a positive constant that trades-off the low-rankness and sparsity.

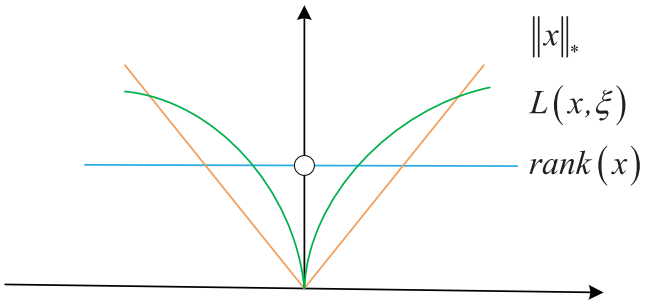

FIGURE 4. Comparison of $L(x,\xi)$, $rank(x)$, $\|x\|_*$ in the case of a scalar.

Use of the nuclear norm as a convex surrogate provides a way to solve the rank minimization problem in the first term of Eq. (14), i.e., rank minimization problem is correct. However, it is very computationally expensive for solution. Inspired the heuristical work in [25], we employ a non-convex optimization toward the rank minimization problem. Instead of the nuclear norm, we use a smooth but non-convex surrogate of the rank. For a given matrix with a symmetric positive semi-definite structure, the rank minimization problem can be approximately surrogate by minimizing the following equation [26]:

$$E(X,\xi) = \log\det(X+\xi I) \tag{18}$$

where ξ is a positive scalar. $E(X,\xi)$ approximates the sum of the logarithm of singular values, thus it is smooth and non-convex. The log det is proved to be a non-convex surrogate of the rank [27]. As shown in Fig. 4, the surrogate function $E(X,\xi)$ yields a better approximate the rank than the nuclear norm.

For the low-rank matrix L, Eq. (15) is rewritten as follows:

$$\begin{aligned} L(L,\xi) &= \log\det((LL^T)^{1/2}+\xi I) \\ &= \log\det(U\Sigma^{1/2}U^{-1}+\xi I) \\ &= \log\det(\Sigma^{1/2}+\xi I) \end{aligned} \tag{19}$$

where Σ is the diagonal matrix whose diagonal elements are eigenvalues of matrix LL^T, i.e.,$LL^T = U\Sigma U^{-1}$; meanwhile, $\Sigma^{1/2}$ is also the diagonal matrix whose diagonal elements are the singular values of the matrix $\mathbf{L}$. Hence, $L(L,\xi)$ is a log det$(\cdot)$ surrogate function of $rank(L)$ obtained by setting $X = \left(LL^T\right)^{1/2}$. Finally, Eq. (14) can be rewritten as follows:

$$(L^*,S^*) = \arg\min_{(L,S)} (L(L,\xi) + \mu\|S\|_1) \quad s.t. F = L+S \tag{20}$$

C. OPTIMIZATION OF THE MODEL

The alternating direction method of multipliers (ADMM) [28] demonstrates a good balance between efficiency and accuracy in solving optimization problems. In this paper, ADMM has been adopted to solve Eq. (17).

The augmented Lagrangian multiplier function of Eq. (17) is as follows:

$$\begin{aligned} L(L,S,Z) = L(L,\xi) + \mu\|S\|_1 + \frac{\beta}{2}\|L+S-F\|_F^2 \\ - \langle Z, L+S-F\rangle \end{aligned} \tag{21}$$

where $Z \in R^{m\times n}$ is the multiplier of the linear constraint, $\beta > 0$ is the penalty parameter for the violation of the linear constraint, $\langle\cdot\rangle$ is the inner product and $\|\cdot\|_F$ is the induced Frobenius norm. The proposed objective function can be solved by alternatively minimizing the objective function with respect to the $\mathbf{L}$, $\mathbf{S}$ and the multiplier $\mathbf{Z}$. It can be described as solving the following three sub-problems:

$$\begin{cases} L^{(k+1)} = \arg\min\limits_{L} L(L^{(k)}, S^{(k)}, Z^{(k)}; \beta) \\ S^{(k+1)} = \arg\min\limits_{S} L(L^{(k+1)}, S, Z^{(k)}; \beta) \\ Z^{(k+1)} = Z^{(k)} - \beta\left(L^{(k+1)} + S^{(k+1)} - F\right) \end{cases} \tag{22}$$

For the first sub-problem in Eq.(19), which solves for $\mathbf{F}$ at fixed $\mathbf{S}$ and $\mathbf{Z}$, it can be explicitly represented as the following form:

$$\begin{aligned} L^* = \arg\min_{L} L(L,\xi) \\ + \frac{\beta}{2}\|L+S-F\|_F^2 - \langle Z, L+S-F\rangle \end{aligned} \tag{23}$$

Substituting Eq.(15) into Eq.(20), we can get the following Equation:

$$\begin{aligned} L^* = \arg\min_{L} \sum_{j=1}^{n_0} L(\sigma_j(L)+\xi) \\ + \frac{\beta}{2}\|L+S-F\|_F^2 - \langle Z, L+S-F\rangle \end{aligned} \tag{24}$$

where $n_0 = \min\{m,n\}$, and $\sigma_j(L)$ indicates the j-th singular value of $\boldsymbol{L}$. For simplicity, we use σ_j to denote $\sigma_j(L)$. Even though $\sum_{j=1}^{n} log(\sigma_j+\xi)$ is non-convex, it can be solved by utilizing a local minimization approach. We define the equality $h(\sigma) = \sum_{j=1}^{n} log(\sigma_j+\xi)$. Then $h(\sigma)$ can be approximated by using its first-order Taylor expansion, as follows:

$$h(\sigma) = h\left(\sigma^{(k)}\right) + \left\langle \nabla h\left(\sigma^{(k)}\right), \sigma - \sigma^{(k)}\right\rangle \tag{25}$$

where $\sigma^{(k)}$ is the solution obtained in the k-th iteration. Therefore, Eq. (21) can be solved by iteratively solving:

$$\begin{aligned} L^{(k+1)} = \arg\min_{L} \frac{\beta}{2}\left\|L^{(k)} + S^{(k)} - F - \frac{Z^{(k)}}{\beta}\right\|_F^2 \\ + \sum_{j=1}^{n} \frac{\sigma_j}{\sigma_j^{(k)}+\xi} \end{aligned} \tag{26}$$

where we use the fact that $\nabla h(\sigma^{(k)}) = \sum_{j=1}^{n_0} \frac{1}{\sigma_j^{(k)}+\xi}$ and ignore the constants in Eq.(22).

In general, for a real matrix, the weighted nuclear norm is a convex function only if the weights are descending, and the optimal solution to Eq.(23) is obtained by a weighted singular value thresholding operator, referred to as the proximal operator. In this paper, the weights are ascending, thus Eq.(23) is non-convex. Therefore, it is difficult to find its global minimizer. Nevertheless, we could find that the weighted singular value thresholding gives one minimizer to Eq.(23) via **Theorem 1** (Proximal Operator of Weighted Nuclear Norm) [29].

Theorem 1 (Proximal Operator of Weighted Nuclear Norm) [29]:

For each $X \in \mathbb{C}^{n\times m}$ and $0 \le \omega_1 \le \cdots \le \omega_{n_0}$, $n_0 = \min\{m, n\}$, a minimizer to

$$\min_L \frac{1}{2}\|X - L\|_F^2 + \tau\varphi(L, \omega) \tag{27}$$

is given by the weighted singular value thresholding operator $\mathcal{S}_{\omega,\tau}(X)$:

$$\mathcal{S}_{\omega,\tau}(X) := U(\Sigma - \tau diag(\omega))_+ V^T \tag{28}$$

where $U\Sigma V^T$ is the SVD of $\mathbf{X}$ and $(x)_+ = \max\{x, 0\}$.

To be consistent with the expression of **Theorem 1**, we convert Eq. (23) into a new form:

$$L^{(k+1)} = \arg\min_L \frac{1}{2}\left\|Y^{(k)} - L^{(k)}\right\|_F^2 + \tau\varphi\left(L, \omega^{(k)}\right) \tag{29}$$

where $\tau = 1/\beta$. $Y^{(k)} = F^{(k)} + \frac{Z^{(k)}}{\beta} - S^{(k)}$, $\varphi(L, \omega) = \sum_j^{n_0} \omega_j^{(k)}\sigma_j$ indicates a weighted nuclear norm whose weights $\omega_j^{(k)} = 1/\left(\sigma_j^{(k)} + \xi\right)$.

According to this **Theorem**, we can obtain the low-rank matrix at the $(k+1)$-th iteration by

$$L^{(k+1)} = U\left(\widetilde{\Sigma} - \tau diag(\omega^{(k)})\right)_+ V^T \tag{30}$$

where $U\widetilde{\Sigma}V^T$ is the SVD of the feature matrix $\mathbf{Y}$, and $\omega_j^{(k)} = 1/\left(\sigma_j^{(k)} + \xi\right)$. Even though the weighted thresholding is only a local minimizer, it always leads to a decrease in the objective function value. In this paper, the initial value $\omega^{(0)}$ is set to $[1, 1, \ldots, 1]^T$.

After solving the low-rank matrix $\mathbf{L}$, the sparse matrix $\mathbf{S}$ can be solved by fixing $\mathbf{L}$ and $\mathbf{Z}$. Indeed, we can easily obtain the solution using the widely-used shrinkage problem [30]:

$$S^{(k+1)} = \frac{1}{\beta}Z^{(k)} - L^{(k+1)} + F - P_{\Omega_\infty^{\gamma/\beta}}\left[\frac{1}{\beta}Z^{(k)} - L^{(k+1)} + F\right] \tag{31}$$

where $P_{\Omega_\infty^{\gamma/\beta}}$ indicates the Euclidean projection onto:

$$\Omega_\infty^{\gamma/\beta} := \left\{X \in R^{n\times n} \,\middle|\, -\gamma/\beta \le X_{ij} \le \gamma/\beta\right\} \tag{32}$$

Then the multipliers $\mathbf{Z}$ can be updated as follows:

$$Z^{(k+1)} = Z^{(k)} - \beta(L^{k+1} + S^{k+1} - F) \tag{33}$$

D. SALIENCY MAP ACQUISITION AND SEGMENTATION

1) SALIENCY MAP ACQUISITION

For a given patterned fabric image, decomposing the feature matrix $\mathbf{F}$ into a low-rank approximation $\mathbf{L}$, which corresponds to the normal patterned background, and a sparse part $\mathbf{S}$, which corresponds to the defective objects. A saliency map $\mathbf{M}$ is generated by the l_1-norm of each column S_i in $\mathbf{S}$, and it is described as follows:

$$M(I_i) = \|S_i\|_1 \tag{34}$$

The larger value of $M(I_i)$ indicates that the patch I_i is more likely to be defective objects.

2) SALIENCY MAP SEGMENTATION

First, obtaining a new saliency map $\hat{M}$ by de-noising the generated saliency map $\mathbf{M}$

$$\hat{M} = g * (M \circ M) \tag{35}$$

where g denotes the radius of circular smoothing filter and "$\circ$" means the Hadamard inner product operator and "$*$" is the convolution operator.

Next, normalizing the new saliency map $\hat{M}$ in [0, 255]

$$\tilde{M} = \frac{\hat{M} - \min(\hat{M})}{\max(\hat{M}) - \min(\hat{M})} \times 255 \tag{36}$$

Finally, segmenting $\tilde{M}$ by adopting an improved adaptive threshold segmentation algorithm [31] to localize the position of defective regions.

IV. EXPERIMENTAL RESULTS

In this section, we evaluate our proposed approach and compare with state-of-the-art methods in the datasets of 256-by-256 patterned fabric images, which are from Industrial Automation Research Laboratory, Dept. of Electrical and Electronic Engineering, The University of Hong Kong, these images have three patterns: star-, box- and dot-patterned fabric datasets for performance validation. There exist 25 defect-free and 25 defective images in the star-patterned fabric dataset, 30 defect-free and 26 defective images in the box-patterned fabric dataset and 110 defect-free and 120 defective images in the dot-patterned fabric dataset, respectively. All the these images have corresponding ground-truth images which are treated as standard criterion. In this paper, all experiments are conducted on the platform of the computer with Inter(R) Core(TM) i3-2120 3.3GHZ CPU and 4G DDR memory, and in the simulation environment of MATLAB 2016a software.

A. QUALITATIVE RESULTS

According to the low-rank decomposition model, the feature matrix extracted from the given patterned fabric image can be divided into the superposition of two parts, i.e., a low-rank approximate matrix and a sparse residual matrix. The final detection result can be obtained from the saliency map which is generated by the sparse matrix, so as to localize the position of the defective regions.

The proposed method includes two parts: feature extraction and detection method, they are equally important for fabric defect detection. In order to validate the effectiveness of our method, we firstly compare the saliency maps generated by different descriptors, including Gabor [23], HOG [32], Gabor+HOG (different from our proposed GHOG, it simply concatenates Gabor and HOG), and HSOG [33] and different detection methods, such as the template matching method (TMM) [34], the context analysis method (CAM) [35] with our method, as shown in Fig. 5.

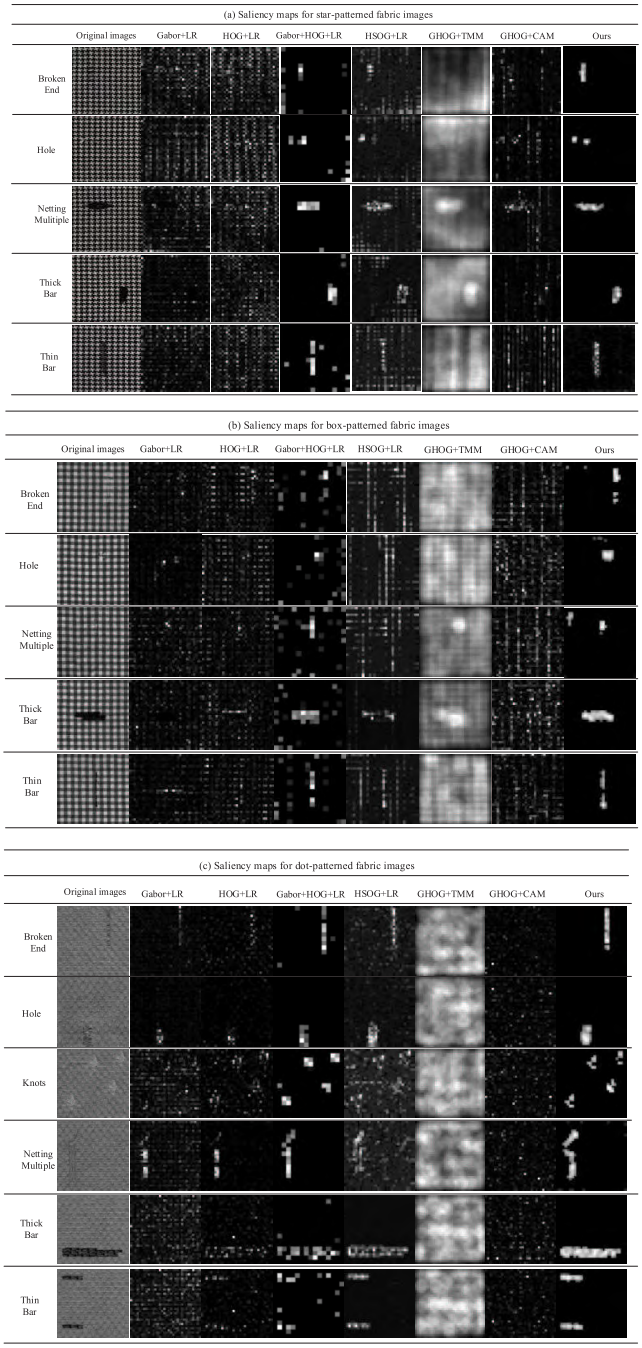

FIGURE 5. The saliency maps generated by different features and detection models. The first column shows the original images, the second column shows saliency maps generated by Gabor [23] with the LR model (Gabor + LR), the third column shows the saliency maps generated by HOG [32] with LR model (HOG + LR), the fourth column shows the saliency maps generated by Gabor and HOG with LR model, the fifth column shows the saliency maps generated by HSOG [33] with LR model (HSOG + LR), the sixth column shows the saliency maps generated by GHOG and TMM model [34] (GHOG + TMM), the seventh column shows the saliency maps generated by GHOG and CAM model [35] (GHOG + CAM), and the last column shows the saliency maps generated by our method.

The first column are the original images, from the second to the seventh column are the saliency maps generated by Gabor feature [23] and the LR detection model, HOG feature [32] and the LR detection model, Gabor+HOG features and the LR detection model, HSOG [33]features and the LR detection model, GHOG feature and the TMM [34] detection model, GHOG feature and the CAM [35] detection model, respectively, and the last column consists of the saliency maps generated by our proposed method (GHOG feature and the LR detection model). From the second column and the fifth column in Fig. 5, we can conclude that the detection results based on the Gabor, HOG and Gabor+HOG and HSOG features combined with LR model cannot outstand the defect region for star-patterned fabric and box-patterned fabric images, but they can outstand the detect region for dot-patterned fabric images. On the other hand, from the sixth column and the seventh column in Fig. 5, the saliency map generated by the GHOG feature and the TMM or CAM detection models cannot outstand the defect region. In the last column, we can see that the saliency map generated by our method can efficiently outstand the defect region for all the three types of images. And the performance of these methods can be concluded as Table 1. From Fig. 5 and Table 1, we can see that the proposed defection method based on GHOG and LR is more suitable for patterned fabric defect detection.

In addition, we compare our method with some state-of-the-art visual saliency models, including WT [36], PGLSR [37], TDVSM [34], LSF-GSA [35] and SOMC [38], as shown in Fig. 6. WT [44] analyzed wavelet coefficients in the frequency domain to obtain the saliency map. However, even in a normal background with complex pattern, its wavelet coefficients are larger, which will lead to incorrect detection results. The PGLSR method [37] could effectively detect defects in the patterned fabric, but similarities in texture between the background and the defect lead to inaccurate shape descriptions of the defects, such as the third image in Fig. 6(a). TDVSM [34] generated the saliency map by computing the subtraction of texture features between each pixels and their average value. It could obtain a better detection performance for fabric images with plain or twill textures, but failed in the patterned fabric defect detection, especially for box-patterned ones. LSF-GSA [35] incorporated local texture features with global analysis to generate saliency map, while the detection results may existed large amount of noises. Our method generates saliency maps by combining the GHOG feature descriptor with a low-rank decomposition model, and it effectively outstands the defective regions. Subsequently, segmenting the generated saliency maps to get the final detection results.

We also compare our detection results with the existing fabric detection algorithm. Since TDVSM [34] is invalid for detecting patterned fabric defect, thus in this work, we only compare the proposed method with the other two valid detection methods,i.e, PGLSR [37] and LSF-GSA [35], the experimental results comparison is described in Fig. 7. In Fig. 7, we can see that the other methods (as shown in the first three columns) can almost localize the defect region, but the detected shape of the defect is different from the ground

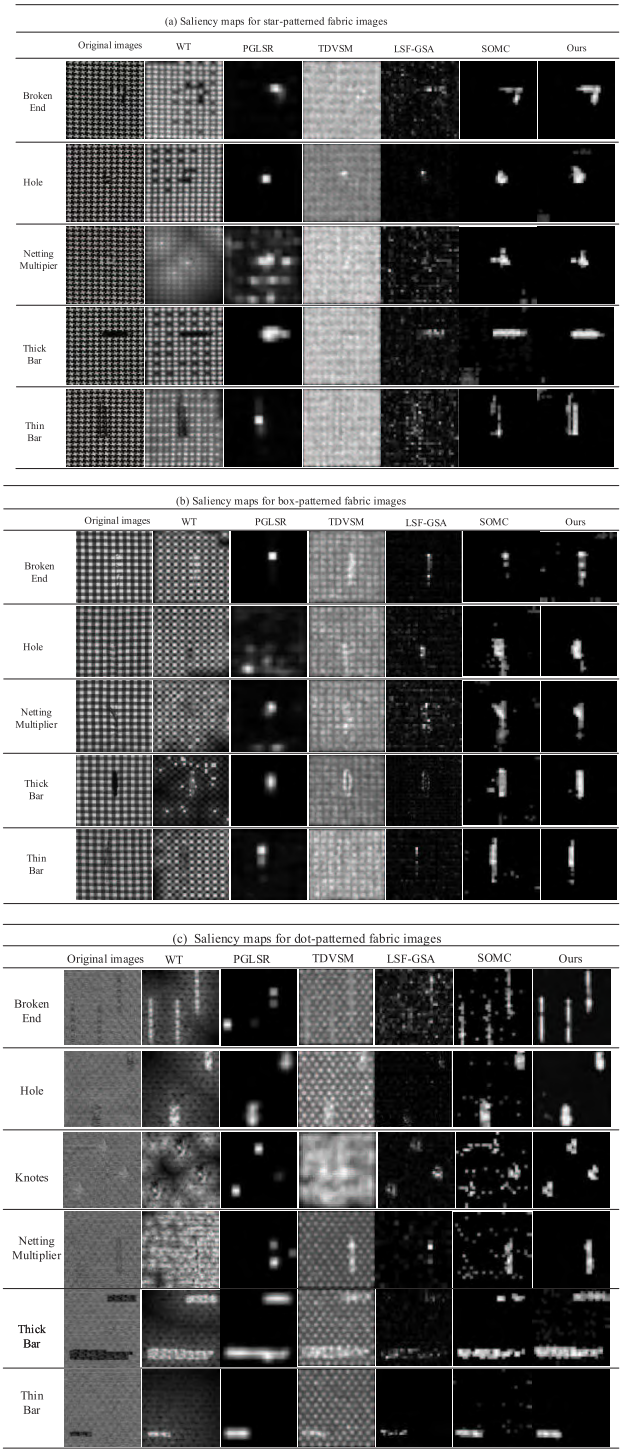

FIGURE 6. The saliency maps of our method compared with other state-of-the-art saliency models. The first column shows the original images, the second column shows saliency maps generated by WT [36], the third column shows the saliency maps generated by PGLSR [37], the fourth column shows the saliency maps generated by TDVSM [34], the fifth column shows the saliency maps generated by LSF-GSA [35], the sixth column shows the saliency maps generated by SOMC [38],and the last column shows the saliency maps generated by our method.

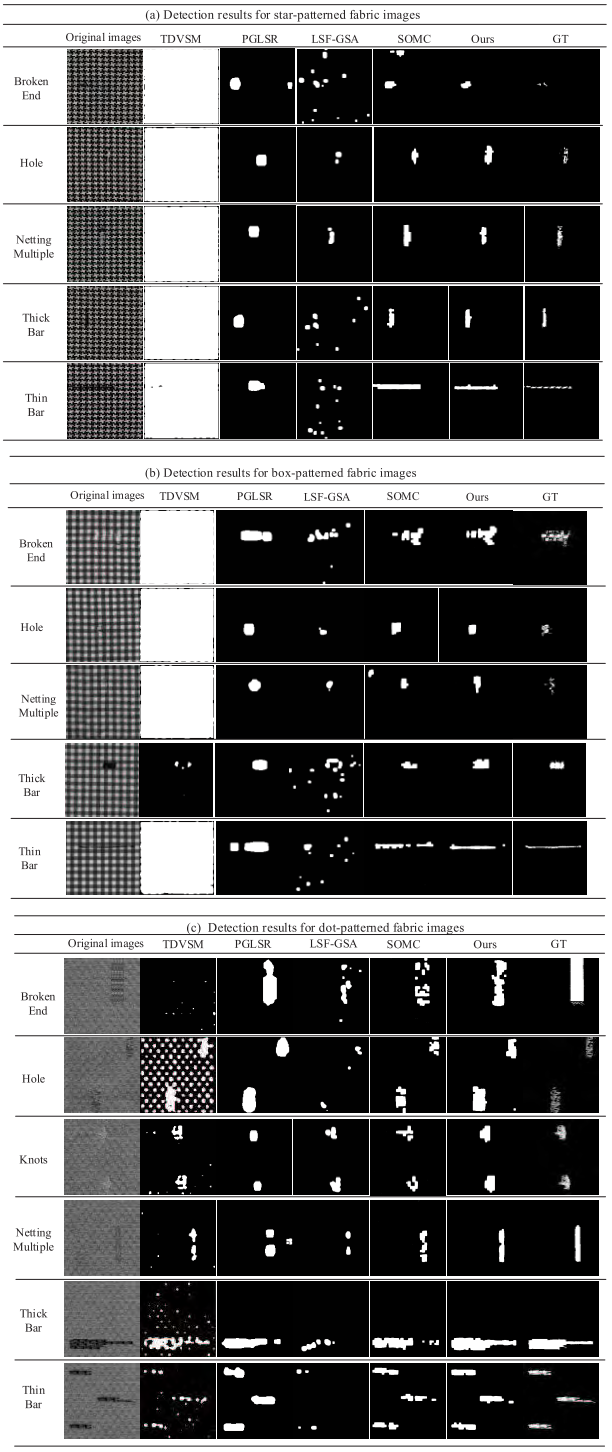

FIGURE 7. Detection results of our method compared with other fabric defect detection methods. The first column shows the original images, the second column shows the detection results of TDVSM [34] method, the third column shows the detection results of PGLSR [37] method, the fourth column shows the detection results of LSF-GSA [35] method, the fifth column shows the detection results of SOMC [38] method,the sixth column shows the detection results of our method, the last column shows the ground-truth images.

truth. Our detection results (as shown in the sixth column) are similar to the ground truth images (as shown in the last column), can efficiently localize the defective regions, and the detected shape of the defect is similar to the ground truth. This demonstrates that our proposed method is superior to the other methods.

TABLE 1. Comparisons with other methods.

Methods/ fabric image	Gabor+LR	HOG+LR	HSOG+LR	GHOG+TMM	GHOG+CAM	GHOG+LR
star-patterned	×	×	√	×	×	√
box-patterned	×	×	×	×	×	√
dot-patterned	√	√	√	×	×	√

TABLE 2. Average numerical results for each defect type of star-patterned fabric images.

Defect / Methods	BrokenEnd					Hole					Netting Multiple					ThickBar					ThinBar				
	ACC(%)	TPR(%)	FPR(%)	PPV(%)	NPV(%)	ACC(%)	TPR(%)	FPR(%)	PPV(%)	NPV(%)	ACC(%)	TPR(%)	FPR(%)	PPV(%)	NPV(%)	ACC(%)	TPR(%)	FPR(%)	PPV(%)	NPV(%)	ACC(%)	TPR(%)	FPR(%)	PPV(%)	NPV(%)
TDVSM [34]	54.45	54.07	45.55	0.82	99.42	57.11	69.99	43.16	3.34	98.89	52.70	67.31	48.35	9.13	95.63	59.65	64.62	41.15	20.18	91.18	57.95	64.39	42.22	3.98	98.35
LSF-GSA [35]	88.37	36.37	8.36	21.41	95.83	91.50	30.33	4.49	30.75	95.43	86.02	23.94	3.97	49.27	88.68	82.53	27.75	8.31	35.83	27.75	88.91	19.34	9.36	4.88	97.84
PGLSR [37]	96.68	45.24	2.60	19.59	99.22	96.59	54.57	2.51	31.88	99.01	92.33	54.57	5.05	42.82	96.79	96.09	60.49	2.07	60.13	97.96	93.78	44.88	4.81	21.25	98.35
SOMC [38]	96.01	65.56	3.65	16.93	99.60	96.96	72.87	2.71	26.81	99.62	95.44	71.99	3.63	44.16	98.86	94.96	67.28	3.29	56.15	97.92	95.77	64.02	3.78	19.07	99.48
WGIS [6]	95.74	0.26	3.56	0.09	99.60	95.82	0.34	3.66	0.05	99.45	94.76	1.03	3.61	0.88	98.25	93.40	4.37	3.44	5.09	96.63	95.42	0	3.65	0	99.00
ER [39]	98.13	8.79	1.16	7.17	99.27	98.32	24.47	1.23	11.68	99.54	97.76	16.42	0.82	12.61	98.54	97.30	69.52	1.67	54.52	98.81	96.72	45.47	2.83	12.50	99.45
BB [18]	98.24	2.83	0.78	3.33	98.99	99.15	2.69	0.16	8.18	99.31	97.60	11.58	0.42	37.11	97.99	96.56	30.67	0.49	63.18	96.88	98.60	6.76	0.23	22.16	98.82
RB [19]	98.75	4.54	**0.45**	7.52	99.19	**99.28**	6.90	**0.12**	25.99	99.39	98.11	15.23	0.25	47.99	98.34	96.79	19.61	**0.32**	77.11	96.86	98.82	3.14	**0.08**	27.69	98.89
ID [40]	97.58	75.62	2.17	17.64	99.74	97.16	72.34	2.69	33.29	99.77	98.75	82.19	0.96	56.60	99.70	**99.30**	94.45	0.47	79.93	99.76	94.98	81.59	4.98	13.86	99.29
GHOG(Proposed)	**99.10**	**76.47**	1.39	**31.61**	**99.76**	98.54	**79.44**	1.12	**36.91**	**99.79**	97.64	70.69	1.24	59.41	99.20	97.26	**95.53**	0.76	**80.50**	99.79	**99.51**	**84.78**	1.40	**37.26**	**99.55**

TABLE 3. Average numerical results for each defect type of box-patterned fabric images.

Defect / Methods	BrokenEnd					Hole					Netting Multiple					ThickBar					ThinBar				
	ACC(%)	TPR(%)	FPR(%)	PPV(%)	NPV(%)	ACC(%)	TPR(%)	FPR(%)	PPV(%)	NPV(%)	ACC(%)	TPR(%)	FPR(%)	PPV(%)	NPV(%)	ACC(%)	TPR(%)	FPR(%)	PPV(%)	NPV(%)	ACC(%)	TPR(%)	FPR(%)	PPV(%)	NPV(%)
TDVSM [34]	41.31	57.24	59.24	3.27	96.46	41.08	62.04	59.08	0.77	99.32	45.17	**65.32**	55.23	2.27	98.50	45.87	**73.88**	56.09	8.44	96.00	42.64	**61.22**	57.54	1.04	99.10
LSF-GSA [35]	89.84	21.56	4.97	24.80	94.10	91.07	32.47	4.80	32.27	95.24	89.15	24.79	7.27	15.91	95.69	85.09	18.54	9.33	14.26	93.00	87.08	23.93	6.27	28.65	92.13
PGLSR [37]	94.24	40.42	2.58	48.04	96.52	90.48	53.93	7.46	29.03	97.26	91.51	28.46	5.09	23.21	96.09	95.28	54.58	2.11	**62.42**	97.11	93.75	44.48	4.51	25.89	97.98
SOMC [38]	94.99	52.16	3.58	32.67	98.37	96.67	62.08	2.81	24.90	99.42	95.18	53.45	3.84	24.74	98.87	94.56	47.56	3.18	41.72	97.47	95.66	57.30	3.73	19.71	99.30
WGIS [6]	74.85	36.39	24.43	2.94	98.40	74.17	31.17	25.52	0.92	99.31	73.77	33.00	25.68	1.28	98.87	75.32	49.08	24.24	4.30	**98.77**	75.33	26.90	24.20	1.02	99.07
ER [39]	95.27	10.26	**0.69**	30.43	95.88	97.66	0	**0.03**	0	97.69	95.77	0.15	**0.04**	4.00	95.81	95.43	22.76	1.68	42.40	96.93	75.33	26.90	24.20	1.02	99.07
GHOG(Proposed)	**95.52**	**57.83**	0.89	**61.44**	**98.57**	**98.26**	**72.37**	0.85	**42.09**	**99.60**	**97.21**	49.88	0.92	**40.67**	**99.02**	**96.69**	47.35	**0.85**	50.41	97.47	**97.71**	57.96	**1.15**	**34.70**	**99.35**

TABLE 4. Average numerical results for each defect type of dot-patterned fabric images.

Defect / Methods	BrokenEnd					Hole					Knots					Netting Multiple					ThickBar					ThinBar				
	ACC(%)	TPR(%)	FPR(%)	PPV(%)	NPV(%)	ACC(%)	TPR(%)	FPR(%)	PPV(%)	NPV(%)	ACC(%)	TPR(%)	FPR(%)	PPV(%)	NPV(%)	ACC(%)	TPR(%)	FPR(%)	PPV(%)	NPV(%)	ACC(%)	TPR(%)	FPR(%)	PPV(%)	NPV(%)	ACC(%)	TPR(%)	FPR(%)	PPV(%)	NPV(%)
TDVSM [34]	46.06	47.84	54.05	5.58	92.95	44.94	52.76	55.21	1.79	98.03	43.16	63.65	57.52	3.54	97.24	46.94	66.97	53.87	4.84	66.97	49.34	57.52	52.31	18.14	84.78	42.62	66.53	57.95	2.68	98.13
LSF-GSA [35]	79.29	21.18	9.58	29.73	85.70	88.91	24.38	4.86	32.62	92.88	87.84	34.78	3.63	60.62	90.19	76.45	17.11	0.99	86.69	75.86	70.58	17.73	2.84	75.83	70.13	90.30	16.23	2.45	39.29	92.25
PGLSR [37]	94.21	31.55	2.09	47.19	96.03	93.79	61.48	4.96	32.53	98.45	94.15	34.36	1.51	62.33	95.38	91.18	25.20	1.37	67.50	92.11	86.46	60.75	4.00	84.92	86.83	94.73	65.61	3.56	52.04	97.95
SOMC [38]	91.77	37.36	3.97	42.43	95.14	93.79	60.35	4.95	31.51	98.45	92.07	45.41	5.15	34.46	96.68	91.58	43.01	4.03	49.04	94.91	87.57	60.45	4.47	79.88	89.17	95.15	64.29	3.16	52.71	98.02
WGIS [39]	80.04	54.93	0.18	25.51	93.90	83.06	75.13	0.17	10.92	99.15	73.55	38.61	0.25	4.89	97.10	81.06	62.92	0.18	14.10	97.73	81.49	71.66	0.17	33.18	95.58	83.39	66.69	0.16	10.66	98.64
ER [39]	96.69	32.27	**0.01**	56.25	91.90	94.49	69.21	**0.05**	30.63	98.94	97.07	54.35	**0.01**	66.88	98.10	96.41	43.79	**0.01**	80.95	97.79	84.76	84.94	**0.15**	49.46	96.19	92.5	81.22	**0.07**	26.81	99.30
BB [18]	87.98	4.46	0.07	76.24	88.00	97.14	26.09	0.63	55.34	96.14	96.77	29.92	0.55	67.93	97.24	96.07	29.43	0.15	90.81	96.14	92.93	63.49	2.88	75.74	94.76	97.21	53.71	1.26	58.67	98.37
RB [19]	88.72	12.33	0.34	64.20	88.65	96.66	15.40	0.72	40.54	95.62	96.40	20.83	0.44	65.78	96.78	95.64	21.15	0.05	**96.39**	95.62	93.72	65.46	2.04	81.43	94.90	97.82	53.93	0.61	75.27	98.37
ID [40]	95.42	68.66	2.00	61.73	96.46	95.62	86.73	4.12	37.00	99.23	98.13	79.47	1.20	69.39	99.24	98.05	85.97	1.30	77.13	99.23	99.57	**98.58**	0.34	97.10	99.86	99.33	97.36	0.59	81.40	**99.91**
GHOG(Proposed)	**97.53**	**76.02**	1.70	**77.72**	**96.98**	**97.90**	**90.19**	2.80	**60.48**	**99.45**	**98.89**	**83.37**	1.74	**71.02**	**99.31**	**98.90**	**88.85**	1.38	53.28	**99.51**	**99.74**	38.44	2.43	**97.56**	84.19	**99.78**	**97.38**	1.53	**85.60**	95.72

B. QUANTITATIVE EVALUATIONS

Some evaluation metrics are introduced to further verify the performance of our approach. Four statistical parameters, i.e., true positive (TP), true negative (TN), false positive (FP), false negative (FN), are adopted in this paper, which have been used by Ng *et al.* [40]. Based on these parameters, some measurement metrics including: Accuracy $ACC = (TP + TN)/(TP + FN + FP + TN)$, true positive rate $TPR = TP/(TP+FN)$, false positive rate $FPR = FP/(FP+TN)$, positive predictive value $PPV = TP/(TP+FP)$ and negative predictive value $NPV = TN/(TN+FN)$. The average numerical results for each defect type of star-, box-, and dot-patterned fabric images are illustrated in Table II, Table 3 and Table IV, respectively. When available, these numerical results of all the compared methods are generated either by using the publicly released source code with fault parameters provided by the authors (including TDVSM [34], PGLSR [37], LSF-GSA) [35], and SOMC [38]), or directly copy the numbers reported in their papers (the results of WGIS [39] and ER [39] are listed in [39] and BB [18], RB [19], and ID [40] are listed in [40]). From these Tables, we can see that our proposed approach performs the best performance on the three benchmark patterned fabric datasets.

C. RUNNING TIME ANALYSIS

In this paper, a non-convex log det as a smooth surrogate function for the rank instead of the nuclear norm is adopted to improve the efficiency of the proposed method. In order to demonstrate its efficiency, we compare the running time for the two methods. For the LR model with nuclear norm, the running time is 0.27 s for detecting one image in our simulation environment; however, the running time for LR model by using smooth surrogate function is 0.18 s. Therefore, our proposed method can efficiently reduce the running time comparing to the traditional low-rank model.

V. CONCLUSION

In this paper, we have presented a novel patterned fabric defect detection method based on GHOG and low-rank decomposition. The main contributions of our method are summarized as follows: 1) in order to efficiently characterize the fabric texture feature, a novel second-order direction-aware feature descriptor, denoted as GHOG, a combination of Gabor and HOG, is proposed; 2) the low-rank decomposition model is adopted for defect detection; 3) in order to improve the efficiency of the proposed method, a non-convex log det as a smooth surrogate function for the rank instead of the nuclear norm is also exploited.

We also compare the performance of the proposed approach with some stae-of-the-art approaches on the three benchmark patterned fabric datasets. Experimental results both in qualitative and quantitative demonstrate the effectiveness and superiority of our proposed approach. Furthermore, our proposed algorithm provides a new idea for surface defect detection of other industrial products.

ACKNOWLEDGMENT

The authors would like to thank Dr. Henry Y.T. Ngan, Industrial Automation Research Laboratory, Dept. of Electrical and Electronic Engineering, The University of Hong Kong, for providing the database of patterned fabric images.

REFERENCES

[1] K. Zhang, Y. Yan, P. Li, J. Jing, X. Liu, and Z. Wang, "Fabric defect detection using salience metric for color dissimilarity and positional aggregation," *IEEE Access*, vol. 6, pp. 49170–49181, 2018.
[2] D. Yapi, M. S. Allili, and N. Baaziz, "Automatic fabric defect detection using learning-based local textural distributions in the contourlet domain," *IEEE Trans. Autom. Sci. Eng.*, vol. 15, no. 3, pp. 1014–1026, Jul. 2018.
[3] S. Susan and M. Sharma, "Automatic texture defect detection using Gaussian mixture entropy modeling," *Neurocomputing*, vol. 239, pp. 232–237, May 2017.
[4] J. Zhou, D. Semenovich, A. Sowmya, and J. Wang, "Dictionary learning framework for fabric defect detection," *J. Textile Inst.*, vol. 105, no. 3, pp. 223–234, 2014.
[5] C. S. C. Tsang, H. Y. T. Ngan, and G. K. H. Pang, "Fabric inspection based on the Elo rating method," *Pattern Recognit.*, vol. 51, pp. 378–394, Mar. 2016.
[6] H. Y. T. Ngan, G. K. H. Pang, S. P. Yung, and M. K. Ng, "Wavelet based methods on patterned fabric defect detection," *Pattern Recognit.*, vol. 38, no. 4, pp. 559–576, 2005.
[7] H. Peng, B. Li, H. Ling, W. Hu, W. Xiong, and S. J. Maybank, "Salient object detection via structured matrix decomposition," *IEEE Trans. Pattern Anal. Mach. Intell.*, vol. 39, no. 4, pp. 818–832, Apr. 2017.
[8] G. Gao, D. Zhang, C. Li, Z. Liu, and Q. Liu, "A novel patterned fabric defect detection algorithm based on GHOG and low-rank recovery," in *Proc. IEEE 13th Int. Conf. Signal Process. (ICSP)*, Nov. 2016, pp. 1118–1123.
[9] M. A. Selver, V. Avşar, and H. Özdemir, "Textural fabric defect detection using statistical texture transformations and gradient search," *J. Textile Inst.*, vol. 105, no. 9, pp. 998–1007, 2014.
[10] S. Guan, T. Zhao, and H. Shi, "Image segmentation of fabric defect based on object rarity feature," *J. Textile Res.*, vol. 36, no. 11, pp. 45–50, 2015.
[11] K. Sakhare, A. Kulkarni, M. Kumbhakarn, and N. Kare, "Spectral and spatial domain approach for fabric defect detection and classification," in *Proc. IEEE Int. Conf. Ind. Instrum. Control (ICIC)*, May 2015, pp. 640–644.
[12] Y. Li, H. Luo, M. Yu, G. Jiang, and H. Cong, "Fabric defect detection algorithm using RDPSO-based optimal Gabor filter," *J. Textile Inst.*, vol. 110, no. 4, pp. 487–495, 2019.
[13] Y. Xiaobo, "Fabric defect detection of statistic aberration feature based on GMRF model," *J. Textile Res.*, vol. 34, no. 4, pp. 137–142, 2013.
[14] M. S. Allili, N. Baaziz, and M. Mejri, "Texture modeling using contourlets and finite mixtures of generalized Gaussian distributions and applications," *IEEE Trans. Multimedia*, vol. 16, no. 3, pp. 772–784, Apr. 2014.
[15] T. Qu, L. Zou, Q. Zhang, X. Chen, and C. Fan, "Defect detection on the fabric with complex texture via dual-scale over-complete dictionary," *J. Textile Inst.*, vol. 107, no. 6, pp. 743–756, 2016.
[16] Q. Zhu, M. Wu, J. Li, and D. Deng, "Fabric defect detection via small scale over-complete basis set," *Textile Res. J.*, vol. 84, no. 15, pp. 1634–1649, 2014.
[17] G. Stübl, J.-L. Bouchot, P. Haslinger, and B. Moser, "Discrepancy norm as fitness function for defect detection on regularly textured surfaces," in *Proc. Joint DAGM, German Assoc. Pattern Recognit., OAGM Symp.* Berlin, Germany: Springer, 2012, pp. 428–437.
[18] H. Y. T. Ngan and G. K. H. Pang, "Novel method for patterned fabric inspection using bollinger bands," *Opt. Eng.*, vol. 45, no. 8, 2006, Art. no. 087202.
[19] H. Y. T. Ngan and G. K. H. Pang, "Regularity analysis for patterned texture inspection," *IEEE Trans. Autom. Sci. Eng.*, vol. 6, no. 1, pp. 131–144, Jan. 2009.
[20] M. K. Ng, H. Y. T. Ngan, X. Yuan, and W. Zhang, "Lattice-based patterned fabric inspection by using total variation with sparsity and low-rank representations," *SIAM J. Imag. Sci.*, vol. 10, no. 1, pp. 2140–2164, 2017.
[21] C. Li, G. Gao, Z. Liu, M. Yu, and D. Huang, "Fabric defect detection based on biological vision modeling," *IEEE Access*, vol. 6, pp. 27659–27670, 2018.
[22] J. Cao, N. Wang, J. Zhang, Z. Wen, B. Li, and X. Liu, "Detection of varied defects in diverse fabric images via modified RPCA with noise term and defect prior," *Int. J. Cloth. Sci. Technol.*, vol. 28, no. 4, pp. 516–529, 2016.
[23] S. E. Grigorescu, N. Petkov, and P. Kruizinga, "Comparison of texture features based on Gabor filters," *IEEE Trans. Image Process.*, vol. 11, no. 10, pp. 1160–1167, Oct. 2002.
[24] M. Brown, G. Hua, and S. Winder, "Discriminative learning of local image descriptors," *IEEE Trans. Pattern Anal. Mach. Intell.*, vol. 33, no. 1, pp. 43–57, Jan. 2011.
[25] Z.-X. Cui and Q. Fan, "A nonconvex nonsmooth regularization method for compressed sensing and low rank matrix completion," *Digit. Signal Process.*, vol. 62, pp. 101–111, Mar. 2017.
[26] M. Fazel, H. Hindi, and S. P. Boyd, "Log-det heuristic for matrix rank minimization with applications to Hankel and Euclidean distance matrices," in *Proc. IEEE Amer. Control Conf.*, vol. 3, Jun. 2003, pp. 2156–2162.
[27] Y. Ma, H. Derksen, W. Hong, and J. Wright, "Segmentation of multivariate mixed data via lossy data coding and compression," *IEEE Trans. Pattern Anal. Mach. Intell.*, vol. 29, no. 9, pp. 1546–1562, Sep. 2007.
[28] K. Guo, D. Han, D. Z. W. Wang, and T. Wu, "Convergence of ADMM for multi-block nonconvex separable optimization models," *Frontiers Math. China*, vol. 12, no. 5, pp. 1139–1162, 2017.
[29] W. Dong, G. Shi, X. Li, Y. Ma, and F. Huang, "Compressive sensing via nonlocal low-rank regularization," *IEEE Trans. Image Process.*, vol. 23, no. 8, pp. 3618–3632, Aug. 2014.
[30] R. Tibshirani, "Regression shrinkage and selection via the lasso," *J. Roy. Statist. Soc. B, Methodol.*, vol. 58, no. 1, pp. 267–288, 1996.
[31] L. Zhoufeng, W. Jiuge, Z. Quanjun, and L. Chunlei, "Research on fabric defect detection algorithm based on improved adaptive threshold," *Microcomput. Appl.*, vol. 32, no. 10, pp. 38–44, 2013.
[32] N. Dalal and B. Triggs, "Histograms of oriented gradients for human detection," in *Proc. IEEE Comput. Soc. Conf. Comput. Vis. Pattern Recognit. (CVPR)*, vol. 1, Jun. 2005, pp. 886–893.
[33] D. Huang, C. Zhu, Y. Wang, and L. Chen, "HSOG: A novel local image descriptor based on histograms of the second-order gradients," *IEEE Trans. Image Process.*, vol. 23, no. 11, pp. 4680–4695, Nov. 2014.
[34] C. Li, Z. Zhang, Z. Liu, L. Liao, and Q. Zhao, "A novel fabric defect detection algorithm based on textural differential visual saliency model," *J. Shandong Univ., Eng. Sci.*, vol. 44, no. 4, pp. 1–9, 2014.
[35] Z. Liu, Q. Zhao, C. Li, Y. Dong, and L. Yan, "Fabric defect detection algorithm using local statistic features and global saliency analysis," *J. Textile Res.*, vol. 35, no. 11, pp. 62–67, 2014.
[36] N. Imamoglu, W. Lin, and Y. Fang, "A saliency detection model using low-level features based on wavelet transform," *IEEE Trans. Multimedia*, vol. 15, no. 1, pp. 96–105, Jan. 2013.
[37] J. Cao, J. Zhang, Z. Wen, N. Wang, and X. Liu, "Fabric defect inspection using prior knowledge guided least squares regression," *Multimedia Tools Appl.*, vol. 76, no. 3, pp. 4141–4157, 2017.
[38] C. Li, C. Liu, G. Gao, Z. Liu, and Y. Wang, "Robust low-rank decomposition of multi-channel feature matrices for fabric defect detection," *Multimedia Tools Appl.*, vol. 78, no. 6, pp. 7321–7339, 2018.
[39] Z.-D. Tsai and M.-H. Perng, "Defect detection in periodic patterns using a multi-band-pass filter," *Mach. Vis. Appl.*, vol. 24, no. 3, pp. 551–565, 2013.
[40] M. K. Ng, H. Y. T. Ngan, X. Yuan, and W. Zhang, "Patterned fabric inspection and visualization by the method of image decomposition," *IEEE Trans. Autom. Sci. Eng.*, vol. 11, no. 3, pp. 943–947, Jul. 2014.

CHUNLEI LI received the B.S. degree in computer science from Zhengzhou University, China, in 2001, the M.S. degree from Hohai University, China, in 2004, and the Ph.D. degree in computer science from Beihang University, China, in 2012. He is currently an Associate Professor with the School of Electronics and Information, Zhongyuan University of Technology. In recent years, he published more than 50 technical papers and has authored two books. He has also obtained three patents. His research interests include machine vision for fabric defect detection, pattern recognition, and low-rank representation.

GUANGSHUAI GAO received the B.Sc. degree in applied physics from the College of Science and the M.Sc. degree in signal and information processing from the School of Electronic and Information Engineering, Zhongyuan University of Technology, Zhengzhou, China, in 2014 and 2017, respectively. He is currently pursuing the Ph.D. degree with the Laboratory of Intelligent Recognition and Image Processing, Beijing Key Laboratory of Digital Media, School of Computer Science and Engineering, Beihang University. His research interests include image processing, pattern recognition, and digital machine learning.

ZHOUFENG LIU received the B.S. degree from Lanzhou University, Lanzhou, China, in 1985, and the M.S. and Ph.D. degrees from the Beijing Institute of Technology, Beijing, China, in 1988 and 1994, respectively. From 1990 to 1995, he was a Lecturer with Zhengzhou University, Zhengzhou, China. From 1998 to 2004, he was an Associate Professor. Since 2004, he has been a Professor with the Zhongyuan University of Technology. His research interests include radar image processing and artificial intelligence. He was the Technical Leader and the Consultation Committee Member of Henan Province.

DI HUANG (S'10–M'11) received the B.S. and M.S. degrees in computer science from Beihang University, Beijing, China, and the Ph.D. degree in computer science from the École centrale de Lyon, Lyon, France, in 2005, 2008, and 2011, respectively. He joined the Laboratory of Intelligent Recognition and Image Processing, Beijing Key Laboratory of Digital Media, School of Computer Science and Engineering, Beihang University, as a Faculty Member. His current research interests include biometrics, in particular, on 2D/3D face analysis, image/video processing, and pattern recognition.

JIANGTAO XI received the B.E. degree from the Beijing Institute of Technology, China, in 1982, the M.E. degree from Tsinghua University, China, in 1985, and the Ph.D. degree from the University of Wollongong, Australia, in 1996, all in electrical engineering. He was a Postdoctoral Fellow with the Communications Research Laboratory, McMaster University, Ontario, Canada, from 1995 to 1996, and a member of Technical Staff with Bell Laboratories, Lucent Technologies Inc., NJ, USA, from 1996 to 1998. He was the Chief Technical Officer with TCL IT Group Company, China, from 2000 to 2002. In 2003, he rejoined the University of Wollongong as a Senior Lecturer, where he is currently a Full Professor and the Head of the School of Electrical, Computer, and Telecommunications Engineering. His research interests include signal processing and its applications in various areas, such as instrumentation and measurement, as well as telecommunications.